

# GRAND: Guidance, Rebalancing, and Assignment for Networked Dispatch in Multi-Agent Path Finding

Johannes Gaber<sup>1,\*</sup>, Meshal Alharbi<sup>1,\*</sup>, Daniele Gammelli<sup>2</sup>, and Gioele Zardini<sup>1</sup>

**Abstract**—Large robot fleets are now common in warehouses and other logistics settings, where small control gains translate into large operational impacts. In this article, we address task scheduling for lifelong Multi-Agent Pickup-and-Delivery (MAPD) and propose a hybrid method that couples learning-based global guidance with lightweight optimization. A graph neural network policy trained via reinforcement learning outputs a desired distribution of free agents over an aggregated warehouse graph. This signal is converted into region-to-region rebalancing through a minimum-cost flow, and finalized by small, local assignment problems, preserving accuracy while keeping per-step latency within a 1s compute budget. On congested warehouse benchmarks from the League of Robot Runners (LoRR) with up to 500 agents, our approach improves throughput by up to 10% over the 2024 winning scheduler while maintaining real-time execution. The results indicate that coupling graph-structured learned guidance with tractable solvers reduces congestion and yields a practical, scalable blueprint for high-throughput scheduling in large fleets.

## I. INTRODUCTION

Large fleets of mobile robots are now common in domains such as autonomous ride-hailing [1] and warehouse automation [2]. At scale, even small coordination gains translate into substantial economic and environmental impacts. For instance, city-scale robotaxi deployments and million-robot fulfillment centers underscore the opportunity for better fleet control [3], [4]. In these systems, a scheduler assigns robots to tasks (i.e., Task Scheduling (TS)) and a planner generates collision-free motions (i.e., Multi-Agent Path-Finding (MAPF)). These two problems are sometimes referred to in the literature as task planning and motion planning, respectively. The warehouse and ride-hailing settings are well captured by Multi-Agent Pickup and Delivery (MAPD), where each task requires visiting two locations in order [5]. The lifelong variants Lifelong Task Scheduling (LTS) and Lifelong Multi-Agent Path-Finding (LMAPF) further model continuous task arrivals. Both scheduling and path finding are known to be NP-hard [6], [7], making exact, monolithic optimization impractical at realistic scales and control rates.

In this context, three families of approaches are prevalent [8]. First, optimization-based schedulers (e.g., Integer Linear Program (ILP)/Hungarian method on A\* distances) provide clean models but can be myopic to congestion and expensive at large scale. Second, heuristics and rules are fast and widely used in practice, yet may leave throughput on the table under heavy coupling. Finally, learning-based methods promise fast inference and the ability to exploit dynamics

<sup>1</sup>Laboratory for Information and Decision Systems, Massachusetts Institute of Technology, Cambridge, MA, USA (e-mails: {jgaber, meshal, gzardini}@mit.edu).

<sup>2</sup>Department of Aeronautics and Astronautics, Stanford University (e-mail: gammelli@stanford.edu).

\*Gaber and Alharbi contributed equally to this work. This work was supported by Prof. Zardini’s grant from the MIT Amazon Science Hub, hosted in the MIT Schwarzman College of Computing.

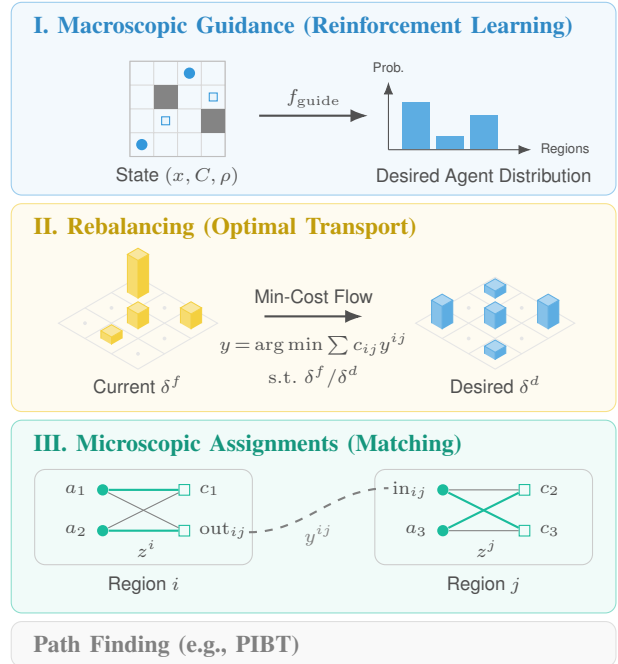


Fig. 1. Overview of GRAND, our hierarchical task scheduling approach: (I) a data-driven layer provides global, macroscopic guidance in the form of a desired agent distribution; (II) a region-to-region optimal transport rebalances free agents toward the desired distribution; and (III) local, decoupled matching problems produce the final assignments for task scheduling. All symbols in the figure are defined later in the text.

beyond simplified models, but often lack guarantees and have struggled to consistently outperform strong heuristics in classic MAPF settings.

*Statement of Contribution:* In this paper, we present a hybrid LTS architecture that cleanly separates *learned global guidance* from *lightweight combinatorial assignment*. A Graph Neural Network (GNN) policy trained with Reinforcement Learning (RL) outputs a desired distribution of free agents over an aggregated warehouse graph; this signal is converted into region-to-region rebalancing via a minimum-cost flow formulation and completed with small, local ILPs, preserving assignment accuracy while keeping per-step latency within a 1s control budget. We call this approach GRAND: a hierarchical algorithm that relies on Guidance, Rebalancing, and Assignment to explicitly leverage the workspace Network structure and Dispatch agents to tasks. Fig. 1 showcases an overview diagram of our methodology. On congested warehouse benchmarks from the League of Robot Runners (LoRR) [9], the resulting scheduler improves throughput by up to 10% over the 2024 winning baseline, demonstrating that coupling graph-structured learned guidance with tractable solvers yields robust, high-throughput control for large fleets.

## II. RELATED WORK

TS in MAPF/MAPD complements collision-aware planning and has been explored mainly via distance-based assignment, heuristics, and learning [8]. When path interactions are ignored, TS reduces to a (possibly unbalanced) weighted bipartite matching between free agents and tasks using A\*-based distances [10]. The resulting assignment can be solved via ILP or the Hungarian method [11], and appears in early MAPD formulations coupling online re-assignment with matching [5]. In congested warehouses, however, distance-optimal allocations at dispatch time need not remain efficient during execution due to conflicts and queuing, motivating faster rules and metaheuristics. For instance, large neighborhood search has been applied to multi-goal MAPD [12]. The LoRR [9] simulator was recently introduced to standardize comparisons for MAPD, providing warehouse-style benchmarks among others. The LoRR has further spurred congestion-aware greedy strategies that perform strongly in practice, including a runner-up based on congestion prediction [13] and the winning 2024 scheduler leveraging refined greedy priorities [14].

Beyond heuristics, a flow-based model that computes a global, system-wide matching between agents and tasks was proposed to guide assignment in sortation centers [15], and several works couple assignment with planning. Chen et al. integrate TS and path planning for capacitated MAPD in a unified framework [16]. Newer variants expand problem scope, e.g., online MAPD with deadlines (MAPD-D) and dynamic path finding for multi-load agents [17]. System-level closed-loop formulations that unify scheduling and planning are also emerging (e.g., FICO [18]). At scale, the LMAPF setting highlights the need for high-quality decisions under tight control budgets and heavy congestion [9].

Learning-based TS and LTS for warehouse MAPD are comparatively sparse [19], especially when compared to the learning-based literature for MAPF [20]. Agrawal et al. employ attention-based RL to directly allocate tasks sequentially [21]. Related large-fleet dispatch domains provide complementary ideas: high-capacity ride-pooling uses graph-structured ILP to jointly assign requests and vehicles [22], while GNN RL has been used to rebalance fleets and improve downstream matching [23], [24], [25]. Our approach follows this hybrid trajectory: learned global guidance on a graph shapes downstream optimization (flow/matching), aiming to capture congestion effects while retaining the reliability and precision of combinatorial solvers, and we evaluate in LoRR’s standardized warehouse environment [9].

## III. BACKGROUND

### A. Reinforcement Learning

RL is a framework for solving sequential decision-making problems that are often modeled as a fully observed Markov Decision Process (MDP). An MDP is characterized by a tuple  $\mathcal{M} = (\mathcal{S}, \mathcal{A}, P, d_0, r, \gamma)$ , where  $\mathcal{S}$  and  $\mathcal{A}$  denote the state and action spaces.  $P(s_{t+1} | s_t, a_t)$  is the transition kernel,  $d_0$  is the initial state distribution,  $r : \mathcal{S} \times \mathcal{A} \rightarrow \mathbb{R}$  is the reward function, and  $\gamma \in (0, 1]$  is the discount factor. A (stochastic) policy  $\pi(a | s)$  maps states to a distribution over actions. For a finite horizon  $H$ , a trajectory is  $\tau = (s_0, a_0, \dots, s_{H-1}, a_{H-1}, s_H)$ , and the probability  $p_\pi(\tau)$  of

this trajectory under policy  $\pi$  is

$$p_\pi(\tau) = d_0(s_0) \prod_{t=0}^{H-1} \pi(a_t | s_t) P(s_{t+1} | s_t, a_t). \quad (1)$$

The RL objective is to find a policy that maximizes the discounted return:

$$J(\pi) = \mathbb{E}_{\tau \sim p_\pi} \left[ \sum_{t=0}^{H-1} \gamma^t r(s_t, a_t) \right]. \quad (2)$$

Data typically come from interacting with the environment using some behavior policy  $\beta$ , often the current version of  $\pi$  under training. Each interaction yields a transition  $(s_t, a_t, r_t, s_{t+1})$ , where  $r_t = r(s_t, a_t)$ , which is used to iteratively improve the policy.

## IV. PROBLEM FORMULATION

We study LTS for multiple agents  $A = \{a_1, \dots, a_N\}$  moving on a directed, reflexive graph  $G = (V, E)$  over discrete timesteps  $t = 0, 1, \dots, T_{\max}$ . Reflexivity encodes the option to wait via self-loops  $(v, v) \in E$ . At each timestep, a scheduler assigns per-agent goals, a planner generates collision-free motions, and a task generator updates completed tasks with new ones. Let  $x_t : A \rightarrow V$  denote the joint position of all agents at time  $t$  (for convenience,  $v_t^a := x_t(a)$ ), and let  $C_t \subseteq V$  denote the set of uncompleted tasks at time  $t$ . We consider a lifelong setting in which the number of available tasks is constant:  $|C_t| = M \in \mathbb{N}$  for all  $t$ .

### A. Mathematical Model

We view  $(x_t, C_t)$  as the system state. Its evolution is governed by the task generator, the scheduling policy, and the planning policy.

**Definition IV.1** (Task generator). A *task generator* is a map  $f_{\text{TG}} : V^A \times 2^V \rightarrow 2^V$  that produces the next task set  $C_{t+1} = f_{\text{TG}}(x_t, C_t)$ . If an agent  $a$  completes a task at time  $t$  (i.e.,  $x_t(a) \in C_t$ ), that task is removed in  $C_{t+1}$  and immediately replaced by a new task. All other tasks carry over from  $C_t$  to  $C_{t+1}$ . This maintains  $|C_{t+1}| = M$ .

In MAPD, a task may comprise an ordered sequence of subgoals completed by a single agent. Now, we formalize our notion of a scheduling policy.

**Definition IV.2** (Goal map). A *goal map* at time  $t$  is an injective map  $\rho_t : A \rightarrow V$ .

**Definition IV.3** (Scheduling policy). A *scheduling policy* is an anytime algorithm  $f_{\text{TS}} : V^A \times 2^V \times V^A \rightarrow V^A$  that, given the current state and the previous goal map, returns a new goal map within a time budget  $b_{\text{TS}} > 0$ :

$$\rho_t = f_{\text{TS}}(x_t, C_t, \rho_{t-1}; b_{\text{TS}}). \quad (3)$$

At  $t = 0$ ,  $\rho_0$  is initialized by the starting position of agents (i.e.,  $\rho_0 = x_0$ ).

For agent  $a$ ,  $\rho_t(a) = c \in C_t$  indicates an assignment to task  $c$ , while  $\rho_t(a) = x_t(a)$  indicates a stay-put command. We require that the goal maps be injective so that no two agents are assigned the same goal (in particular, not the same task). The goal maps are used as the interface between the scheduling and planning policies.

**Definition IV.4** (Planning policy). A *planning policy* is an anytime algorithm  $f_{\text{PP}} : V^A \times V^A \rightarrow V^A$  that takes a system state and a goal map and returns a new joint position:

$$x_{t+1} = f_{\text{PP}}(x_t, \rho_t; b_{\text{PP}}), \quad (4)$$

where  $b_{\text{PP}} > 0$  is a time budget for planning.  $f_{\text{PP}}$  is constrained such that for all  $a \in A$ ,  $(x_t(a), x_{t+1}(a)) \in E$ , and the transition  $(x_t, x_{t+1})$  is collision-free in the standard MAPF sense (no vertex collisions or swap conflicts).

The planner seeks to optimize the agents' paths while guaranteeing deadlock avoidance. We refer the reader to Li et al. [18] for formal definitions of collisions and conflicts in MAPF. The objective in the LTS problem we study in this article is the maximization of throughput.

**Definition IV.5** (Throughput). The *throughput*  $\alpha$  is defined as the total number of tasks completed by all agents over the horizon  $T_{\text{max}}$ . Because the task generator immediately replaces completed tasks, we can write:

$$\alpha = \sum_{t=0}^{T_{\text{max}}} \sum_{a \in A} \mathbf{1}_{\{x_t(a) \in C_t\}}. \quad (5)$$

*Real-Time Execution:* We target real-time settings (e.g., warehouse fleets) with a fixed per-timestep time budget of 1 s shared by scheduling and planning policies:

$$b_{\text{TS}} + b_{\text{PP}} \leq 1 \text{ s}. \quad (6)$$

At each timestep  $t$ , the scheduler  $f_{\text{TS}}$  computes  $\rho_t$  within  $b_{\text{TS}}$  and the planner  $f_{\text{PP}}$  updates  $x_{t+1}$ . Movements are executed and  $C_{t+1}$  is updated by the task generator  $f_{\text{TG}}$ . The problem is initialized by specifying a valid starting position  $x_0$  and an initial task set  $C_0$ .

### B. Problem Configuration

The TS model above admits a broad family of configurations parametrized by the tuple  $(G, |A|, M, f_{\text{TG}}, f_{\text{PP}})$ . In this work, we instantiate  $G$  as a warehouse-style layout: a two-dimensional, four-connected grid over traversable *aisle* cells, with shelving modeled by removing blocked cells from  $V$ ; edges may be directed to encode one-way aisles, and self-loops  $(v, v) \in E$  encode waiting.

To summarize load and spatial density, we use two dimensionless ratios:

$$r_{\text{task/agent}} = \frac{M}{|A|}, \quad r_{\text{agent/node}} = \frac{|A|}{|V|}.$$

The task-to-agent ratio  $r_{\text{task/agent}}$  measures *task pressure* per agent: when  $r_{\text{task/agent}} > 1$ , a persistent backlog is inevitable, and new tasks cannot all be assigned immediately. Conversely,  $r_{\text{task/agent}} \leq 1$  allows instantaneous assignment in principle. The agent-to-node ratio  $r_{\text{agent/node}}$  captures *occupancy*: sparse, lightly loaded regimes (low  $r_{\text{agent/node}}$ ) yield weak coupling and few conflicts; dense regimes (high  $r_{\text{agent/node}}$ ) induce strong coupling, making both scheduling and collision-aware planning critical for throughput. Directed aisles can mitigate head-on conflicts but increase path asymmetry, further amplifying the role of the planner at higher densities [26]. Our study will explore this design space by sweeping  $(|A|, M)$  for fixed  $G$ ,  $f_{\text{TG}}$ , and  $f_{\text{PP}}$ , covering sparse-to-dense and under- to over-saturated regimes.

## V. METHODOLOGY

We decompose TS into three stages: (i) a data-driven *global guidance* that prescribes a desired distribution of *free agents* across aggregated regions; (ii) a region-to-region *rebalancing* step that solves an optimal transport problem to route agent mass toward the desired distribution; and (iii) *specific task assignments* obtained by solving decoupled local ILPs consistent with the rebalancing flow.

We operate on an aggregated graph defined by a seed set  $V_{\text{agg}} \subseteq V$ . Each node  $v \in V$  is mapped to its aggregate region  $\pi(v) \in V_{\text{agg}}$  (e.g., Voronoi partition over seeds, with a fixed tie-breaker). Region  $i \in V_{\text{agg}}$  thus represents the cell  $\{v \in V : \pi(v) = i\}$ .

### A. Global Guidance

Rather than outputting an assignment directly (i.e., a mapping between free agents and free tasks), the guidance layer produces a low-dimensional intermediate target that shapes TS. Let  $A_t^f \subseteq A$  be the set of *free agents* at time  $t$  (i.e., agents eligible to receive a new goal) and let  $N_t := |A_t^f|$ . We define the map from the current system state to a distribution as:

$$f_{\text{guide}} : V^A \times 2^V \times V^A \rightarrow \Delta(V_{\text{agg}}) \\ (x_t, C_t, \rho_{t-1}) \mapsto \delta_t^d,$$

where  $\Delta(V_{\text{agg}}) = \{\delta \in \mathbb{R}_+^{|V_{\text{agg}}|} : \sum_i \delta(i) = 1\}$  is the probability simplex over regions. We interpret  $\delta_t^d$  as the *desired distribution* of free agents across regions. The current free-agent distribution is

$$\delta_t^f(i) = \frac{|A_t^f \cap \{a : \pi(x_t(a)) = i\}|}{N_t} \in \Delta(V_{\text{agg}}). \quad (7)$$

If  $\delta_t^d$  matches the (normalized) distribution of free tasks per region, the method reduces to a greedy assignment; when  $\delta_t^d$  shifts mass toward regions with few current tasks, it induces proactive rebalancing (e.g., anticipating arrivals or alleviating congestion).

### B. Rebalancing

Given the desired distribution  $\delta_t^d \in \Delta(V_{\text{agg}})$  from the global guidance step and the current distribution  $\delta_t^f \in \Delta(V_{\text{agg}})$  of free agents, the second step computes a flow  $y_t$  that transports  $\delta_t^f$  to  $\delta_t^d$  at minimum cost. We define the integer supplies  $n_i^s = N_t \delta_t^f(i)$  (cf. Eq. (7)) and the integer demands  $n_i^d = N_t \delta_t^d(i)$  (after suitable rounding that ensure  $\sum_i n_i^d = N_t$ ) for all regions  $i \in V_{\text{agg}}$ . We model rebalancing as a balanced transportation problem on a *complete* bipartite graph, where left and right node sets are both copies of  $V_{\text{agg}}$  and the distances  $c_{ij} \in \mathbb{Z}_{\geq 0}$  between nodes  $i, j \in V_{\text{agg}}$  are the shortest-path distances in  $G$ . Then, the flow  $y_t$  is the solution to the following optimization problem:

$$\min_{y_t} \sum_{i \in V_{\text{agg}}} \sum_{j \in V_{\text{agg}}} c_{ij} y_t^{ij} \quad (8)$$

$$\text{s.t.} \quad \sum_{j \in V_{\text{agg}}} y_t^{ij} = n_i^s, \quad \forall i \in V_{\text{agg}}, \quad (9)$$

$$\sum_{i \in V_{\text{agg}}} y_t^{ij} = n_j^d, \quad \forall j \in V_{\text{agg}}, \quad (10)$$

$$y_t^{ij} \in \mathbb{Z}_{\geq 0}, \quad \forall i, j \in V_{\text{agg}}. \quad (11)$$

The decision variables  $y_t^{ij}$  represent the number of agents rebalanced from region  $i$  to region  $j$ , and we write  $y_t = (y_t^{ij})_{i,j \in V_{\text{agg}}}$ . Since this is a balanced transportation problem with integer supplies, demands, and costs, an optimal integer flow  $y_t$  exists and can be computed efficiently using standard multi-source multi-sink minimum-cost flow solvers [27].

### C. Local Task Assignments

Given the region-to-region flow  $y_t$  from the rebalancing step, we compute the goal map  $\rho_t$  by solving  $|V_{\text{agg}}|$  *decoupled* local problems, one per region  $i \in V_{\text{agg}}$ . The local problem determines which real agents in region  $i$  (i) satisfy the required outflows to other regions and (ii) are assigned to real tasks in  $i$  consistent with the inflows routed to  $i$ . Let

$$A_i^f = \{a \in A : a \text{ is free at } t \text{ and } \pi(x_t(a)) = i\},$$

$$C_i^f = \{c \in C_t : \pi(c) = i\},$$

be the *real* free agents and free tasks in region  $i$ . Recall that  $y_t^{ij}$  is the number of free agents to be routed from  $i$  to  $j$ . We denote the total outflow and inflow for region  $i$  by

$$\text{out}_i := \sum_{j \in V_{\text{agg}}} y_t^{ij}, \quad \text{in}_i := \sum_{j \in V_{\text{agg}}} y_t^{ji}.$$

Note that a *self-flow*  $y_t^{ii}$  represents agents that remain in  $i$ .

To avoid coupling across regions, cross-region interactions are represented by placeholders located at region seeds:

- For each *outgoing* flow  $y_t^{ij}$  with  $j \neq i$ , create an *artificial task set*  $C_j^{\text{out}}$  with  $|C_j^{\text{out}}| = y_t^{ij}$ , all located at the seed node of region  $j$ . Intuitively, matching a real agent in  $i$  to one of these tasks instructs it to travel to  $j$ .
- For each *incoming* flow  $y_t^{ji}$  with  $j \neq i$ , create an *artificial agent set*  $A_j^{\text{in}}$  with  $|A_j^{\text{in}}| = y_t^{ji}$ , all located at the seed node of region  $j$ . Intuitively, matching such a placeholder to a real task in  $i$  reserves that task for an agent traveling from  $j$ .

We then aggregate the local sets as:

$$A_i = A_i^f \cup \left( \bigcup_{j \neq i} A_j^{\text{in}} \right), \quad C_i = C_i^f \cup \left( \bigcup_{j \neq i} C_j^{\text{out}} \right).$$

For any  $a \in A_i$  and  $c \in C_i$ , let  $w_{ac} \in \mathbb{Z}_{\geq 0}$  denote their directed shortest-path distance in  $G$  (for placeholders we use seed-to-node distances; these can be precomputed).

*Local optimization (region  $i$ ):* We formulate a minimum-cost bipartite matching problem:

$$\min_{z^i} \sum_{a \in A_i} \sum_{c \in C_i} w_{ac} z_t^{i,ac} \quad (12)$$

$$\text{s.t.} \quad \sum_{c \in C_i} z_t^{i,ac} \leq 1, \quad \forall a \in A_i, \quad (13)$$

$$\sum_{a \in A_i} z_t^{i,ac} \leq 1, \quad \forall c \in C_i, \quad (14)$$

$$\sum_{a \in A_i^f} z_t^{i,ac} = 1, \quad \forall c \in \bigcup_{j \neq i} C_j^{\text{out}}, \quad (15)$$

$$\sum_{a \in A_i} \sum_{c \in C_i} z_t^{i,ac} = \kappa_i, \quad (16)$$

$$z_t^{i,ac} \in \{0, 1\}, \quad \forall (a, c) \in A_i \times C_i. \quad (17)$$

Here,  $z_t^{i,ac}$  indicates whether agent  $a$  is matched to task  $c$ , and  $\kappa_i = \min(|A_i|, |C_i|)$  is the local matching size. Constraint (15) enforces that every *outgoing* placeholder is fulfilled by a *real* agent currently in  $i$ ; equivalently, artificial agents cannot be matched to artificial tasks, preventing spurious cross-region matches. The remaining constraints are standard assignment constraints. Because the constraint matrix is totally unimodular, the LP relaxation already yields integral solutions; the problem can be solved as a min-cost flow or with the Hungarian algorithm after adding dummies to make it square [28].

**Remark V.1** (Feasibility and interpretation). Since the rebalancing step conserves free agents, we have  $\sum_i \text{out}_i = \sum_i \text{in}_i = N_t$ , and for each  $i$ , the supply constraint guarantees  $\text{out}_i = |A_i^f|$  (recall supplies are derived from actual free-agent counts). Thus, the number of outgoing placeholders in  $i$  equals  $|A_i^f|$ , and (15) is feasible. Self-flow  $y_t^{ii}$  is handled implicitly: those agents are matched to *real* tasks in  $C_i^f$  or are unmatched (i.e., they remain within  $i$  without a task).

*Recovering the global goal map:* After solving (12)–(17) for all  $i \in V_{\text{agg}}$ :

- 1) If a *real agent*  $a \in A_i^f$  is matched to a *real task*  $c \in C_i^f$ , set  $\rho_t(a) = c$ .
- 2) If a *real agent*  $a_i$  in region  $i$  is matched to an outgoing placeholder corresponding to flow from  $i$  to  $j$ , and an incoming placeholder corresponding to flow from  $i$  to  $j$  is matched to a *real task*  $c_j$  in region  $j$  (cf. Fig. 1), we set  $\rho_t(a_i) = c_j$ . When multiple agents traverse the same pair  $(i, j)$ , we pair the list of  $a_i$ 's with the list of  $c_j$ 's using a distance-based greedy procedure that iteratively matches each agent to the nearest currently unassigned reserved task in  $j$ .

Any real agent that remains unmatched to a real task receives a waypoint at its designated destination region, ensuring a well-defined goal for every free agent.

## VI. METHOD DETAILS

In this section, we spell out the components used by our scheduler: (i) a graph aggregation that partitions the workspace into a small number of regions while preserving shortest-path structure; (ii) a data-driven guidance map  $f_{\text{guide}}^d$  learned with RL that outputs a desired distribution  $\delta_t^d$  over regions; and (iii) the rebalancing and local assignment procedures described in Section V-B and Section V-C. Here, we focus on how we construct  $V_{\text{agg}}$ , define the state and action spaces for learning, and implement the guidance policy.

### A. Graph Aggregation

Given a graph  $G = (V, E)$ , the aggregation step chooses *seed* nodes  $V_{\text{agg}} \subseteq V$  and assigns every node  $v \in V$  to one region via a shortest-path Voronoi partition. Let  $\text{dist}_G(u, w)$  denote the (directed) shortest-path distance in  $G$  (finite on our warehouse layouts). We define the regional map

$$\pi(v) \in \arg \min_{i \in V_{\text{agg}}} \text{dist}_G(v, i),$$

breaking ties by a fixed, deterministic rule (e.g., lowest seed index), so that the regions  $\{V_i := \{v \in V : \pi(v) = i\}\}_{i \in V_{\text{agg}}}$  form a partition of  $V$ .

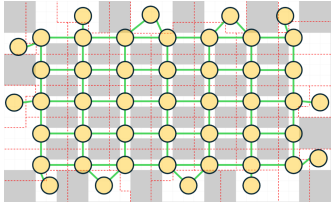


Fig. 2. An example of our graph aggregation for warehouse layouts.

On dense warehouse layouts, we populate  $V_{\text{agg}}$  with: (i) all aisle intersections (i.e., to capture routing hubs/bottlenecks), and (ii) perimeter pick/pack stations (i.e., to capture sinks/sources). This yields regions aligned with traffic structure while preserving geodesic distances in  $G$  (including directed one-way aisles and waiting self-loops). In typical instances, this aggregation reduces the number of vertices (i.e., from  $|V|$  to  $|V_{\text{agg}}|$ ) by more than 90%. We show an example of this aggregation in Fig. 2. More generally, seeds can be chosen by overlaying a coarse, approximately uniform grid on the map.

### B. Global Guidance via Reinforcement Learning

We learn a guidance map  $f_{\text{guide}}$  that outputs a desired regional distribution  $\delta_t^d \in \Delta(V_{\text{agg}})$ . A data-driven approach via GNN RL lets us adapt to arbitrary graphs  $G$ , planning policies  $f_{\text{PP}}$ , task generators  $f_{\text{TG}}$ , and performance metrics.

*a) State Representation:* We build a sparse neighborhood graph  $G_{\text{nh}} = (V_{\text{agg}}, E_{\text{nh}})$  over the aggregate regions. An ordered pair  $(i, j) \in E_{\text{nh}}$  is included when the directed geodesic distance in  $G$  is below a threshold  $\varepsilon > 0$ , i.e.,  $(i, j) \in E_{\text{nh}} \iff \text{dist}_G(i, j) \leq \varepsilon$ , so  $G_{\text{nh}}$  inherits directionality from  $G$  (one-way aisles remain asymmetric). Given the system state  $(x_t, C_t)$  and the previous goal map  $\rho_{t-1}$ , a feature map

$$f_{\text{feature}} : V^A \times 2^V \times V^A \rightarrow (\mathbb{R}^{m_v})^{V_{\text{agg}}} \times (\mathbb{R}^{m_e})^{E_{\text{nh}}},$$

produces per-node and per-edge features that serve as the RL state  $s_t \in \mathcal{S}$ . Node features summarize local load, capacity, and context: we include counts of agents, free agents, tasks, and free tasks currently in region  $i$ , normalized by  $|V_i|$  or by the number of free agents  $N_t$  for scale invariance. Further, we include a congestion proxy given by the fraction of unoccupied nodes in  $V_i$  (clipped to  $[0, 1]$ ), a short-horizon estimate of incoming and outgoing flow based on the previous goal map, and sinusoidal encodings of the region's spatial position together with a time encoding to disambiguate symmetries and capture periodic demand. Edge features capture travel and cross-region interaction: we use the directed geodesic length  $\ell_{ij} = \text{dist}_G(i, j)$  together with its bounded reciprocal  $1/(1 + \ell_{ij})$ . Further, we consider a demand-supply hint equal to the number of free tasks in  $j$  that are closer (in  $G$ ) to free agents in  $i$  than any other agents, normalized by  $|V_j|$ , and a corridor-load statistic computed along a representative shortest path from  $i$  to  $j$  (e.g., mean or maximum occupancy, again clipped to  $[0, 1]$ ).

*b) Algorithm and Policy Representation:* We train the guidance policy with Soft Actor Critic (SAC) [29], a model-free, off-policy RL algorithm with entropy regularization. The (parameterized) actor  $f_{\text{actor}}^\theta : \mathcal{S} \rightarrow \mathcal{A}$  maps the RL state to the RL action space  $\mathcal{A} := \mathbb{R}_+^{|V_{\text{agg}}|}$ . For a state  $s_t \in \mathcal{S}$ ,

we interpret the output of the actor  $f_{\text{actor}}^\theta(s_t) = a_t$  as a concentration parameter for a Dirichlet distribution  $\text{Dir}(a_t)$ , where each sample  $\alpha \sim \text{Dir}(a_t)$  is a valid probability vector (i.e.,  $\alpha \in \Delta(V_{\text{agg}})$ ). During training, SAC keeps the actor stochastic, while at deployment, we operate based on  $\mathbb{E}_{\alpha \sim \text{Dir}(a_t)}[\alpha]$ . Because  $s_t$  is defined on the neighborhood graph  $G_{\text{nh}}$ , both actor and critic share a graph-aware encoder: a transformer-style graph network (i.e., attention with neighborhood masking [30]) followed by per-node MLPs. The critic includes an additional permutation-invariant aggregation (sum/mean pooling) to obtain a global embedding before the value head. The critic  $f_{\text{critic}}^\theta : \mathcal{S} \times \mathcal{A} \rightarrow \mathbb{R}$  thus consumes  $(s_t, a_t)$  and estimates  $Q(s_t, a_t)$ .

*c) Reward Design:* The guidance policy is trained with a shaped reward that balances immediate completions and proximity to completion. Let  $D_t = \{c \in C_t : \exists a \in A \text{ s.t. } x_t(a) = c\}$  be the set of tasks finished at time  $t$  (cf. throughput in Section IV-A). The completion term is  $r_t^{\text{fin}} = |D_t|$  (optionally normalized by  $|A|$  for scale invariance). To mitigate sparsity-pronounced at high  $r_{\text{task/agent}}$  or  $r_{\text{agent/node}}$ , we add a progress term that rewards states in which assigned tasks are close to finishing. Let  $A_t^{\text{act}} = \{a \in A : \rho_t(a) \in C_t\}$  denote the set of agents actively assigned to a task at time  $t$  and  $\tau_t(a) := \min_{\tau \geq t : x_\tau(a) = \rho_t(a)}$  denote the first completion time. We set  $r_t^{\text{fut}} = \sum_{a \in A_t^{\text{act}}} \phi(\tau_t(a) - t)$  with  $\phi(t) = 1/(1 + t)$  or  $\phi(t) = e^{-t/\kappa}$ , so  $r_t^{\text{fut}}$  is large when many active assignments are near completion. We delay enqueueing the transition  $(s_t, a_t, r_t, s_{t+1})$  into the replay buffer until  $r_t^{\text{fut}}$  is available (i.e., after observing a long enough trace of  $x_t$ ). The final reward is a weighted sum  $r_t = c_1 r_t^{\text{fin}} + c_2 r_t^{\text{fut}}$ , with  $c_1, c_2 > 0$  chosen by a grid search on a validation set.

### C. Optimization Solver

Both the global rebalancing in Section V-B and the local assignments in Section V-C are implemented with off-the-shelf minimum-cost flow / bipartite matching solvers on their *linear* relaxations.

*a) Global Rebalancing:* We pose rebalancing as a balanced transportation problem on the complete graph over  $V_{\text{agg}}$ , with  $|V_{\text{agg}}|$  supply/demand nodes and  $|V_{\text{agg}}|^2$  arcs. Standard min-cost flow algorithms solve this in  $O(|V_{\text{agg}}|^3)$  time in the worst case.

*b) Local Assignment:* The matching stage decomposes across regions  $i \in V_{\text{agg}}$ . Let  $n_i := \max\{|A_i|, |C_i|\}$ . After padding to an  $n_i \times n_i$  cost matrix, each regional problem is solvable in  $O(n_i^3)$  time (e.g., Hungarian) or as a small min-cost flow instance with identical complexity guarantees. These subproblems are *fully parallelizable* across regions; with sufficient workers, the wall-clock time is dominated by the largest region:

$$\text{serial: } O(|V_{\text{agg}}|^3 + \sum_i n_i^3), \quad \text{parallel: } O(|V_{\text{agg}}|^3 + \max_i n_i^3).$$

## VII. CASE STUDY

To validate our method and compare it to the state-of-the-art, we perform a case study on different warehouse scenarios in simulation.

### A. Environment

We use LoRR [9] as the environment for all numerical results. LoRR provides a simulation engine for MAPF and TS, enabling fair comparisons across algorithms. The simulator in LoRR assumes a discrete-time, 4-neighbor grid with heading-constrained motion, where at each step an agent may rotate in place, move forward one cell, or wait. Tasks in LoRR require an agent to visit two locations (errands) in order (i.e., MAPD). Agents may be *reassigned* to a different task provided they have not yet started the first errand.

The LoRR effort also includes an annual competition in which teams submit new algorithms for MAPF and TS. For the planning policy  $f_{PP}$ , we use the Traffic-Flow Guided PIBT (TFGP) algorithm [31], the default planner in the 2024 LoRR competition. For the task generator  $f_{TG}$ , we uniformly sample new tasks from the set of unoccupied nodes at time  $t$ . Throughout, we report the number of tiles  $|V_{\text{tile}}|$  as the size of the graph  $G$ . A tile corresponds to a node in the discretized environment and may be either traversable (e.g., warehouse pathways) or non-traversable (e.g., shelves). Unless stated otherwise,  $T_{\text{max}} = 10,000$ . The remaining parameters ( $|V_{\text{tile}}|, |A|, M$ ) vary across figures.

**Remark VII.1** (Success rate). In all tested scenarios, we ensure sufficient time for the planner  $f_{PP}$  to return a valid plan. As a result, we do not evaluate regimes of extreme congestion that may induce deadlocks, which would primarily reflect properties of the planner rather than the scheduler.

### B. Benchmarks

The 2024 LoRR competition concluded in March 2025, with 22 teams participating in the TS track. We compare against three baselines. First, LORR WINNER, the winning TS entry by team *No Man’s Sky* [14], is a heuristic that ranks agent-task pairs using a customized cost metric. Second, G-OPT, a *global* minimum-cost matching between all free agents and available tasks, where edge costs are shortest-path distances. Although the problem is posed as an ILP, we solve its linear relaxation, which is tight for assignment and yields an integral optimum (equivalently solvable by the Hungarian method). Finally, GREEDY, the default greedy assignment implemented in LoRR [9]. We refer to these methods as LORR WINNER, G-OPT, and GREEDY.

### C. Training and Compute

We train the RL guidance map  $f_{\text{guide}}$  with a horizon  $T_{\text{max}} = 150$ . Training converges in roughly 2,000 episodes (around 24 hours wall-clock) on a single NVIDIA Quadro RTX 8000 (48 GB VRAM). With our choice of  $\epsilon$ , the RL graph is highly connected, containing about 90% of the edges of the corresponding complete graph. Empirically, using a shorter horizon with more episodes stabilizes learning and improves final performance. For evaluation, *all methods* are executed under an identical compute budget: an AMD Ryzen 7 5825U CPU (single-threaded) with 16 GB RAM. To ensure fairness, we neither parallelize the local assignment step nor run  $f_{\text{guide}}$  on a GPU during evaluation.

### D. Throughput

Fig. 3 reports throughput as a function of the number of agents  $|A|$  and map size  $|V_{\text{tile}}|$ . Across all configurations

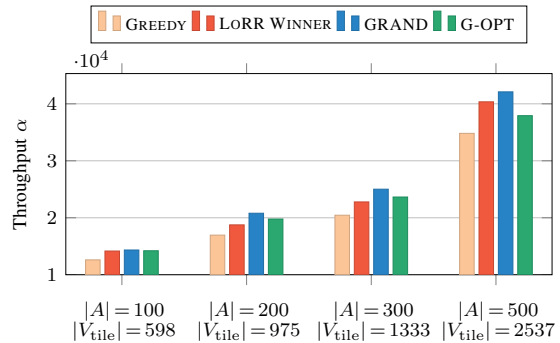


Fig. 3. Throughput for varying numbers of agents  $|A|$  and map sizes  $|V_{\text{tile}}|$ .

TABLE I  
THROUGHPUT FOR 200 AGENTS AND A MAP SIZE OF 975.

Method	Without Reassignment	With Reassignment
GREEDY	12372	16952
LORR WINNER	12990	18752
GRAND	<b>17916</b>	<b>20752</b>
G-OPT	16554	19781

we fix the environment parameters to  $r_{\text{task}/\text{agent}} = 1.5$  and  $r_{\text{agent}/\text{node}} = 0.35$ . For our method, we train a separate policy for each  $(|A|, |V_{\text{tile}}|)$  using a single set of hyperparameters. Our algorithm outperforms all benchmarks at every scale: relative to LORR WINNER, the average gains are about 10% on the two medium instances and 4.3% on the largest instance. When we consider a more restrictive setting in which TS algorithms are not permitted to reassign tasks, the performance gap between our algorithm and competing methods widens, as shown in Table I.

To probe the source of these gains, Table II decomposes the average *time-to-task* (i.e., time to reach the first errand) and *time-in-task* (i.e., time from the first to the second errand) for  $|A| = 200$  and  $|V_{\text{tile}}| = 975$ . The results indicate that higher throughput does not arise from merely dispatching the nearest free agents. Instead, agents complete assigned tasks faster under our TS policy, pointing to reduced congestion. We quantify congestion by counting how often the planner  $f_{PP}$  must deviate from its preferred path and execute a lower-priority action (i.e., a *conflict*). Fig. 4 visualizes this conflict density for our method and for LORR WINNER. On this instance, our method reduces the peak number of conflicts by 23% and the total number of conflicts by 20%, consistent with the observed throughput improvements. Finally, in Table III, we report throughput across a range of map topologies beyond warehouses. The results show that our method remains competitive across diverse environments.

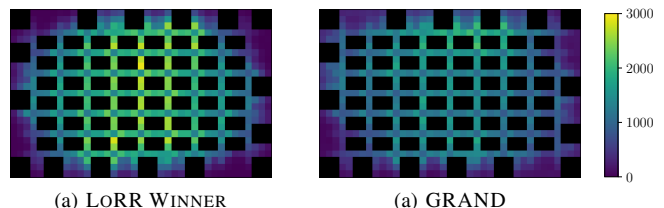


Fig. 4. Number of total conflicts for  $(|A|, |V_{\text{tile}}|) = (200, 975)$ .

TABLE II

THROUGHPUT, TIME-TO-TASK, AND TIME-IN-TASK FOR 200 AGENTS.

Metric	GREEDY	LoRR WINNER	GRAND	G-OPT
Throughput	16952	18752	<b>20752</b>	19781
Time-to-task	32.6 s	16.1 s	24.0 s	<b>10.2 s</b>
Time-in-task	86.9 s	88.5 s	<b>70.9 s</b>	90.6 s

TABLE III

THROUGHPUT ACROSS DIFFERENT MAP TOPOLOGIES.

Map	GREEDY	LoRR WINNER	GRAND	G-OPT
Room ( $ A  = 200$ )	10993	12561	<b>14912</b>	13801
Maze ( $ A  = 400$ )	1508	2013	<b>2417</b>	2062

### E. Scheduling Time

In Fig. 5, we compare the TS per-step computation times across different scales. Specifically, we distinguish between the initial steps in the environment, where all agents are unassigned, and the lifelong (steady state) steps, where the population of free agents and open tasks stabilizes. As expected, optimization-based baselines incur higher latency than heuristic methods. In steady state, our approach dedicates over 90% of the 1 s control-cycle budget to the planner  $f_{PP}$  and still runs substantially faster than the global matching baseline G-OPT. For large deployments, wall-clock can be further reduced through engineering, via accelerators for the guidance module (e.g., TPU/ASIC) and parallelization of the local assignment step, while keeping the evaluation setting otherwise unchanged.

### F. Adaptability

Because our approach involves learning, we evaluate *zero-shot* transfer: train on a single configuration and test on different instances *without* retraining or tuning. Fig. 6 probes sensitivity to the ratio  $r_{\text{agent/node}}$ , Fig. 7 probes sensitivity to graph size  $|V_{\text{tile}}|$ . Across both stressors, our TS policy adapts to unseen settings and, in most cases, continues to outperform the state-of-the-art LoRR WINNER baseline. Notably, performance is competitive even when the evaluation conditions depart substantially from the training configuration, indicating that the learned guidance captures transferable structure

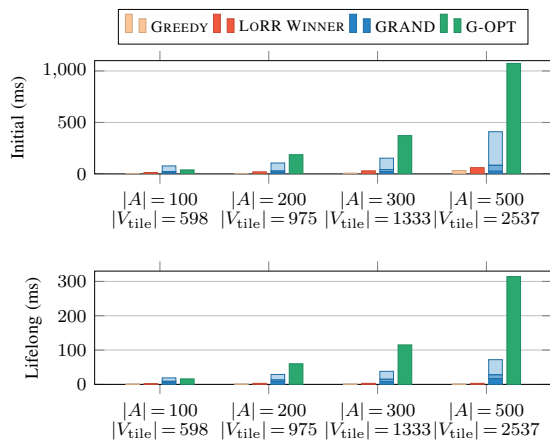


Fig. 5. Average initial and lifelong per-step computation times. For our method, the darkest shade represents the guidance step, the medium shade the rebalancing step, and the lightest shade the matching step.

TABLE IV

ABLATION OF THE DIFFERENT STEPS IN OUR METHOD. EVALUATION WITH 200 AGENTS AND A MAP SIZE OF 975 WITHOUT REASSIGNMENT.

Metric	GRAND	Guidance			Matching Greedy
		Uniform	Demand	Random	
Throughput	<b>17916</b>	16433	14910	14281	14476
Time-to-task	<b>27.1 s</b>	35.5 s	32.7 s	38.5 s	69.3 s
Time-in-task	<b>83.9 s</b>	85.8 s	101.1 s	101.6 s	68.4 s

rather than overfitting to a single regime.

### G. Ablation

In Table IV, we present an ablation study of the key components of our method. For the guidance step, we replace the RL distribution with (i) a uniform distribution over nodes, (ii) a demand distribution formed by normalizing the number of free tasks at each node, or (iii) a random Dirichlet distribution with parameter  $\alpha = 0.1$ . The RL distribution outperforms all three alternatives. Notably, the uniform distribution yields throughput comparable to the global optimization baseline. Intuitively, uniform guidance imposes no directional bias on agent movements, reducing our framework to a linear assignment problem. Even with weakened guidance, the system remains well-behaved, since feasibility and collision avoidance are enforced downstream rather than in the learned component. For the matching step, we replace the decoupled linear assignment problems with a flow-constrained greedy matching. While this improves over the unguided greedy baseline GREEDY (cf. Table I), it incurs a substantial drop in throughput relative to our matching procedure described in Section V-C.

## VIII. CONCLUSION

We proposed a hybrid task-scheduling architecture that pairs a learned, global guidance policy with a lightweight optimization layer for precise agent-task assignment. This separation yields higher throughput across scales, with gains attributable to reduced congestion, while keeping per-step latency well within a 1 s control budget and below the global matching baseline G-OPT. The policy also transfers zero-shot across occupancy ratios and map sizes without tuning. Beyond results, the approach highlights the value of graph neural representations for warehouse-like, graph-structured environments, providing compact and transferable inductive bias for large fleets and maps.

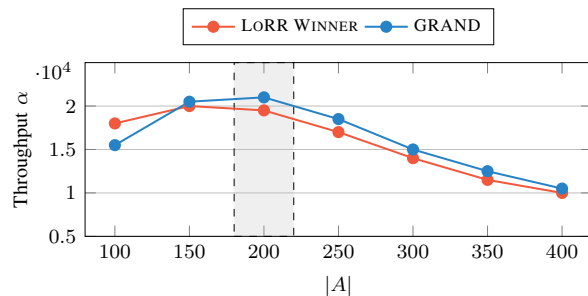


Fig. 6. Throughput for  $|V_{\text{tile}}| = 975$ . Our method is trained on  $|A| = 200$  and deployed on the other instances without retraining.

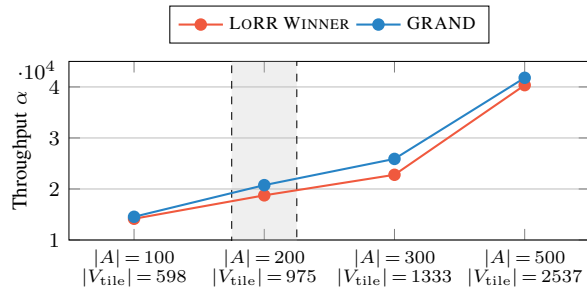


Fig. 7. Throughput for different scales. Our method is trained on the shaded instance and deployed on the other instances without retraining.

**Limitations and outlook:** Key directions include: (i) co-design with path planning via joint learning to further reduce congestion; (ii) closing sim-to-real gaps via log-driven calibration and improved disturbance modeling, with explicit safety constraints to support deployment of GRAND on real systems; (iii) scaling to heterogeneous agents/tasks, time windows, and priorities, with parallelism/accelerators for guidance and local assignment; and (iv) developing theory on stability, sample efficiency, and performance bounds for the hybrid RL–optimization scheme.

In summary, learning-based global guidance coupled with optimization-based local assignment offers a practical, scalable blueprint for real-time, high-throughput scheduling in classical and lifelong MAPF/MAPD, and a foundation for co-designed task–motion systems at industrial scale.

## REFERENCES

- [1] G. Zardini, N. Lanzetti, M. Pavone, and E. Frazzoli, “Analysis and Control of Autonomous Mobility-on-Demand Systems,” *Annual Review of Control, Robotics, and Autonomous Systems*, vol. 5, no. 1, pp. 633–658, 2022.
- [2] R. D’Andrea, “Guest Editorial: A Revolution in the Warehouse: A Retrospective on Kiva Systems and the Grand Challenges Ahead,” *IEEE Transactions on Automation Science and Engineering*, vol. 9, no. 4, pp. 638–639, 2012.
- [3] J. Elias and L. Kolodny, “Waymo Reports 250,000 Paid Robotaxi Rides per Week in U.S.” 2025, <https://www.cnbc.com/2025/04/24/waymo-reports-250000-paid-robotaxi-rides-per-week-in-us.html>.
- [4] S. Dresser, “Amazon Launches a New AI Foundation Model to Power its Robotic Fleet and Deploys its 1 Millionth Robot,” 2025, <https://www.aboutamazon.com/news/operations/amazon-million-robots-ai-foundation-model>.
- [5] H. Ma, J. Li, T. Kumar, and S. Koenig, “Lifelong Multi-Agent Path Finding for Online Pickup and Delivery Tasks,” in *Proceedings of the 16th Conference on Autonomous Agents and MultiAgent Systems*, 2017.
- [6] J. Yu and S. LaValle, “Structure and Intractability of Optimal Multi-Robot Path Planning on Graphs,” in *Proceedings of the AAAI Conference on Artificial Intelligence*, vol. 27, 2013, pp. 1443–1449.
- [7] M. Döring, J. Fehse, T. Friedrich, P. Marten, N. Mohrin, K. Simonov, F. Soheil, J. Timm, and S. Verma, “Parameterized Complexity of Vehicle Routing,” *arXiv preprint arXiv:2509.10361*, 2025.
- [8] L. Antonyshyn, J. Silveira, S. Givigi, and J. Marshall, “Multiple Mobile Robot Task and Motion Planning: A Survey,” *ACM Computing Surveys*, vol. 55, no. 10, pp. 1–35, 2023.
- [9] S.-H. Chan, Z. Chen, T. Guo, H. Zhang, Y. Zhang, D. Harabor, S. Koenig, C. Wu, and J. Yu, “The League of Robot Runners Competition: Goals, Designs, and Implementation,” in *ICAPS 2024 System’s Demonstration track*, 2024.
- [10] P. E. Hart, N. J. Nilsson, and B. Raphael, “A Formal Basis for the Heuristic Determination of Minimum Cost Paths,” *IEEE Transactions on Systems Science and Cybernetics*, vol. 4, no. 2, pp. 100–107, 1968.
- [11] L. Ramshaw and R. E. Tarjan, “On Minimum-Cost Assignments in Unbalanced Bipartite Graphs,” *HP Labs, Palo Alto, CA, USA, Tech. Rep. HPL-2012-40R1*, vol. 20, p. 14, 2012.
- [12] Q. Xu, J. Li, S. Koenig, and H. Ma, “Multi-Goal Multi-Agent Pickup and Delivery,” in *2022 IEEE/RSJ International Conference on Intelligent Robots and Systems (IROS)*. IEEE, 2022, pp. 9964–9971.
- [13] Y. Gao, H. Ding, Y. Wang, J. Zhang, Q. Sun, Q. Zhang, Y. Huang, M. Luo, Z. Su, J. Ding et al., “Adaptive Congestion-Based Algorithms for Multi-Goal Task Assignment and Path Finding in Large-Scale Multi-Agent Systems,” *The League of Robot Runners Virtual Expo 2025*, 2025.
- [14] E. Yuhnevich and A. Andreychuk, “Enhancing PIBT via Multi-Action Operations,” *arXiv preprint arXiv:2511.09193*, 2025.
- [15] N. M. Kou, C. Peng, H. Ma, T. S. Kumar, and S. Koenig, “Idle Time Optimization for Target Assignment and Path Finding in Sortation Centers,” in *Proceedings of the AAAI Conference on Artificial Intelligence*, vol. 34, 2020, pp. 9925–9932.
- [16] Z. Chen, J. Alonso-Mora, X. Bai, D. D. Harabor, and P. J. Stuckey, “Integrated Task Assignment and Path Planning for Capacitated Multi-Agent Pickup and Delivery,” *IEEE Robotics and Automation Letters*, vol. 6, no. 3, pp. 5816–5823, 2021.
- [17] H. Makino and S. Ito, “Online Multi-Agent Pickup and Delivery with Task Deadlines,” in *2024 IEEE/RSJ International Conference on Intelligent Robots and Systems (IROS)*. IEEE, 2024, pp. 8428–8434.
- [18] J. Li, A. Zanardi, R. Zhang, and G. Zardini, “FICO: Finite-Horizon Closed-Loop Factorization for Unified Multi-Agent Path Finding,” *arXiv preprint arXiv:2511.13961*, 2025.
- [19] H. Wang, W. Ye, J. Wang, and W. Chen, “Breaking the Hierarchy: Taxonomies and Survey on Multi-robot Integrated Task and Motion Planning,” *techriv preprint techriv.173933261.11143776*, 2025.
- [20] S. Wang, H. Xu, Y. Zhang, J. Lin, C. Lu, X. Wang, and W. Li, “Where Paths Collide: A Comprehensive Survey of Classic and Learning-Based Multi-Agent Pathfinding,” *arXiv preprint arXiv:2505.19219*, 2025.
- [21] A. Agrawal, A. S. Bedi, and D. Manocha, “RTAW: An Attention Inspired Reinforcement Learning Method for Multi-Robot Task Allocation in Warehouse Environments,” in *2023 IEEE International Conference on Robotics and Automation (ICRA)*. IEEE, 2023, pp. 1393–1399.
- [22] J. Alonso-Mora, S. Samaranayake, A. Wallar, E. Frazzoli, and D. Rus, “On-Demand High-Capacity Ride-Sharing via Dynamic Trip-Vehicle Assignment,” *Proceedings of the National Academy of Sciences*, vol. 114, no. 3, pp. 462–467, 2017.
- [23] D. Gammelli, K. Yang, J. Harrison, F. Rodrigues, F. C. Pereira, and M. Pavone, “Graph Neural Network Reinforcement Learning for Autonomous Mobility-on-Demand Systems,” in *2021 60th IEEE Conference on Decision and Control (CDC)*. IEEE, 2021, pp. 2996–3003.
- [24] D. Gammelli, J. Harrison, K. Yang, M. Pavone, F. Rodrigues, and F. C. Pereira, “Graph Reinforcement Learning for Network Control via Bi-Level Optimization,” in *International Conference on Machine Learning*. PMLR, 2023, pp. 10587–10610.
- [25] L. Tresca, C. Schmidt, J. Harrison, F. Rodrigues, G. Zardini, D. Gammelli, and M. Pavone, “Robo-taxi Fleet Coordination at Scale via Reinforcement Learning,” *arXiv preprint arXiv:2504.06125*, 2025.
- [26] H. Zang, Y. Zhang, H. Jiang, Z. Chen, D. Harabor, P. J. Stuckey, and J. Li, “Online Guidance Graph Optimization for Lifelong Multi-Agent Path Finding,” in *Proceedings of the AAAI Conference on Artificial Intelligence*, vol. 39, 2025, pp. 14726–14735.
- [27] P. Kovács, “Minimum-Cost Flow Algorithms: An Experimental Evaluation,” *Optimization Methods and Software*, vol. 30, no. 1, pp. 94–127, 2015.
- [28] D. Bertsekas, *Network Optimization: Continuous and Discrete Models*. Athena Scientific, 1998, vol. 8.
- [29] T. Haarnoja, A. Zhou, P. Abbeel, and S. Levine, “Soft Actor-Critic: Off-Policy Maximum Entropy Deep Reinforcement Learning with a Stochastic Actor,” in *International Conference on Machine Learning*. PMLR, 2018, pp. 1861–1870.
- [30] Y. Shi, Z. Huang, S. Feng, H. Zhong, W. Wang, and Y. Sun, “Masked Label Prediction: Unified Message Passing Model for Semi-Supervised Classification,” in *Proceedings of the Thirtieth International Joint Conference on Artificial Intelligence*, 2021.
- [31] Z. Chen, D. Harabor, J. Li, and P. J. Stuckey, “Traffic Flow Optimization for Lifelong Multi-Agent Path Finding,” in *Proceedings of the AAAI Conference on Artificial Intelligence*, vol. 38, no. 18, 2024, pp. 20674–20682.